

Date of publication xxxx 00, 0000, date of current version xxxx 00, 0000.

Digital Object Identifier 10.1109/ACCESS.2024.0429000

Derived Power Streams for Fault Detection and Condition-Based Maintenance

AARON W. LANGHAM¹, (Graduate Student Member, IEEE), THOMAS C. KRAUSE¹, (Graduate Student Member, IEEE) and STEVEN B. LEEB¹, (Fellow, IEEE)

¹Massachusetts Institute of Technology, Cambridge, MA 02139 USA

Corresponding author: Aaron W. Langham (e-mail: alangham@mit.edu).

ABSTRACT Nonintrusive electrical monitoring enables fault detection and diagnostics for power systems from an aggregate monitoring point. Faulty electromechanical equipment often produces unrecognizable electrical signatures that confound data-driven techniques. Fault signatures are typically unknown during training. For some loads, analytical models and simulation can predict fault signatures, facilitating their inclusion in the training set. However, this approach scales unfavorably with the number of parameters associated with faults. An alternate outlook recognizes that faults often change the power system conditions and the quality of power delivered. Assumptions about the character and quality of the local grid should be called into question during faulty load behavior. The objectives of this work are to correlate these changing grid behaviors with load and fault signatures as a step towards automatic fault detection. Our methodology involves creating supplemental “derived” data streams distilled from nonintrusive electrical measurements that can correlate changes in grid conditions and quality with load operation. Using real fault data from shipboard microgrids, our key findings illustrate that combining these derived streams with nonintrusive power data enables both nonintrusive load identification and fault diagnosis. Finally, this work presents a vision for implementing an integration of these streams with physics-based fault models in an automatic fault detection system.

INDEX TERMS Fault detection, nonintrusive load monitoring, power quality, smart metering

NOMENCLATURE

CBM	Condition-based maintenance.
DFT	Discrete Fourier transform.
$i_A(t)$	Phase A time-domain current.
I_A	Phase A current spectral envelope.
LG fault	Single line-ground fault.
LLG fault	Double line-ground fault.
MCS	Machinery control system.
NILM	Nonintrusive load monitor.
RMS	Root mean square.
THD	Total harmonic distortion.
USCGC	US Coast Guard cutter.
$v_{AB}(t)$	Line-to-line time-domain voltage from phase B to phase A.
V_{AB}	Line-to-line voltage spectral envelope from phase B to phase A.
VUF	Voltage unbalance factor.

I. INTRODUCTION

Timely detection of electrical faults is important for user safety, energy conservation, and monetary savings. Power

monitoring provides value across all kinds of energy systems and enables fault detection and condition-based maintenance (CBM). A faulty load often will present an evolving energy consumption profile. This can take forms such as short cycling, gradually changing power consumption, and discrete changes in electrical signature. A large body of work has demonstrated that a nonintrusive load monitor (NILM) can provide these benefits with a minimally invasive sensor profile [1]–[3]. However, techniques for CBM using a NILM have typically assumed that the power system’s topology and conditions are modeled correctly. Stated another way, NILM techniques typically ascribe anomalous electrical behavior to faulty load operation and assume generation and distribution systems are healthy. This assumption breaks down when the monitored power system’s conditions change. For example, variations in the generation lineup on microgrids alter the amplitude and frequency of the utility voltage waveform. Accordingly, this alters the electrical behavior of distribution and loads. Preprocessing techniques can compensate or correct for these deviations when used in data-driven pipelines [4]. A gap remains, however, in applying data-driven analysis with a

NILM to local power systems where the *topology*, rather than simply the parameters, of the utility and distribution systems have changed. Traditional NILM-based fault detection methods are insufficient when grid conditions no longer match the conditions encountered in a NILM's training dataset.

This work adapts the spectral envelope framework used by NILMs in literature to recognize these types of fault scenarios. Nonintrusive load monitoring can in principle be applied to power networks of any size and topology, such IEEE 13-bus [5] and 57-bus test systems [6]. However, the scope of this work includes standalone power systems (such as microgrids) rather than interconnected systems. Several examples of system faults demonstrate the utility of indicator streams derived from aggregate electrical measurements. Beyond detecting anomalous system behavior, modern machine learning and fault detection tools can be informed by classical power system techniques. A NILM can correlate these indicators to observed system operation to aid fault detection. In some cases, a NILM can compensate load electrical signatures to align with their profile on a "healthy" grid. This work presents case studies of these techniques on both simulated data and data from real-world shipboard microgrids. The contributions of this work are as follows:

- Spectral envelope adaptations of well understood power quality indicator streams.
- Case studies in which a NILM can correlate these indicators to observed system operation to aid fault detection.
- Field data from real-world shipboard microgrids demonstrating the value of these techniques for fault detection.

II. NONINTRUSIVE FAULT DETECTION

Electromechanical load degradation, both gradual and sudden, may be difficult or impossible for watchstanders to detect. Automatic control exacerbates this issue by scheduling load operation to meet setpoints regardless of load condition. However, degraded load behavior often shows up plainly in the load's power consumption. In a typical polyphase ac grid installation, a NILM samples the currents and voltages on each phase at an upstream location in the power network. By doing so it has access to the power system's aggregate electrical signature, which contains all downstream electrical behavior. Current and voltage data contains some amount of noise and distortion. Preprocessing techniques that use the windowed discrete Fourier transform (DFT) are typically applied to enhance the resolution of the power signature [7]. From this aggregate signature, a NILM can disaggregate the individual electrical signatures of loads connected downstream. A wealth of load disaggregation techniques exists in literature, as reviewed in [8]. Disaggregation techniques can generally be described as either event-based or non-event-based [9]. Non-event-based techniques process a data point or window of electrical data and infer the states of downstream electrical loads using classifiers such as hidden Markov models or neural networks. By contrast, this work focuses on event-based disaggregation, which finds each electrical "event" and infers the load (or loads) responsible.

Derived Stream	Ideal for	Less applicable to
$ I_0 $	Delta grids Wye grids without neutral	Wye grids with neutral
VUF	High source impedance grids	Low source impedance grids
THD	Grids with power electronics	Grids with linear loads

TABLE 1. Derived stream applicability across grid types.

The NILM identifies transitions in power consumption (referred to as "events") and matches them to known load state changes (such as "OFF" to "ON"). This matching can be performed with a data-driven pattern classifier of any desired complexity, from simple correlation scoring to deep neural networks. Regardless of which technique it uses, a practical NILM requires training data that generalizes well to actual load behavior.

Faulty electrical behavior typically results in "out of distribution" inference, where the observed data is no longer well covered by the training data [10]. Multiple techniques to address this problem have been presented in literature. For example, if a fault is gradual enough, a NILM may be able to recognize and even track the associated drifting electrical signatures [11]. This only applies for loads with "soft" faults, in which degradation happens gradually over time. In addition, faults often lead to unidentifiable electrical signatures. With additional context, such as the expected sequence of load state changes, an electrical event's identity may be able to be inferred [12]. For sudden faults that occur on physically simple loads, circuit models with parameterized faults can generate electrical signatures for a wide variety of fault conditions [13]. Exhaustive enumeration and simulation over a large number of failure cases and parameters augments a NILM's training data for a given load. However, this increases the computational cost of both training and inference. Also, this modeling approach may not be available for every load of interest.

An alternate approach recognizes that when loads fail, they often change the conditions of the power system and the quality of the power flow. This paper demonstrates that a NILM can compute "derived streams" of information that characterize a microgrid power system's condition. Correlating these streams with observed load operation extends load recognition and diagnostics to faulty electrical signatures. Additionally, the derived streams quantify a fault's effect on the microgrid power distribution system.

III. DERIVED STREAMS

Ancillary data streams from extra hardware can supplement traditional NILM measurements of voltages and currents, and assist with load analysis [14]. Examples of these streams include vibration, acoustic emission, temperature, and current harmonics. Streams generated in software from manipulated electrical measurements are also informative. Examples include drift scores for evolving load behavior [11] and electrical resolution based on current noise floors in the power sys-

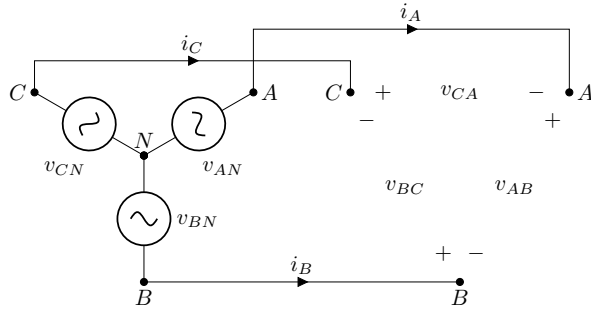


FIGURE 1. Example three-phase ac grid circuit diagram, showing line-to-line voltages and line currents.

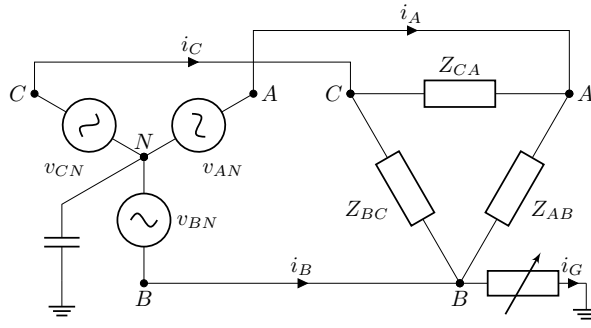


FIGURE 2. Ungrounded power system with a capacitively connected line-ground (LG) fault from phase B to ground.

tem [7]. Naturally, a NILM can also produce derived streams for power system analysis with classical, well-understood techniques [15], [16]. This section presents three case studies in which abnormal grid behavior seen by a NILM is clarified using derived electrical streams. Table 1 shows an overview of these three derived streams, and their applicability across grids.

Consider an ungrounded three-phase ac grid operating at 60 Hz and 440 V rms (measured line-to-line), whose circuit diagram is shown in Figure 1. A NILM on this system samples the phase currents ($i_A(t)$, $i_B(t)$, and $i_C(t)$) and the line-to-line voltages ($v_{AB}(t)$, $v_{BC}(t)$, and $v_{CA}(t)$) at 8 kHz. From these measurements, the NILM identifies the voltage zero crossings and then computes spectral envelopes with the DFT for each current and voltage waveform [17]. Spectral envelopes are used in this work because they preserve fast electrical transients by computing envelope values over only one utility cycle (e.g., 16.7 ms on a 60 Hz grid or 20 ms on a 50 Hz grid). By only saving in-phase and quadrature values at the fundamental frequency and harmonics of interest (such as 3rd, 5th, and 7th), the data rate is drastically reduced from the raw data. This alleviates much of the burden in data storage, retrieval, and processing. In addition, spectral envelopes at the fundamental frequency naturally provide an instantaneous phasor estimation of the waveform, allowing spectral envelopes to be used in a wide variety of ac system

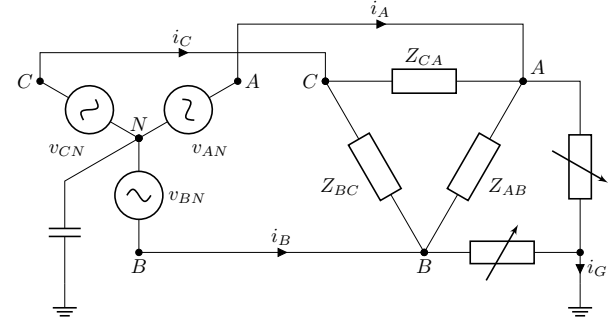


FIGURE 3. Ungrounded power system with a capacitively connected double line-ground (LLG) fault from phases A and B to ground.

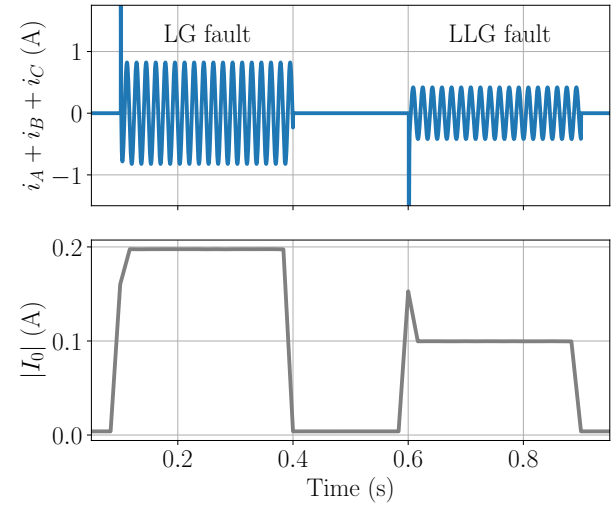


FIGURE 4. Two representations of ground fault current. The top figure shows the sum of i_A , i_B , and i_C . The bottom figure shows the magnitude of the zero-sequence current phasor ($|I_0|$). A single line-to-ground fault occurs at $t = 0.1$ s, increasing $|I_0|$ by 0.2 A above its baseline value of 0 A. A double line-to-ground fault occurs at $t = 0.6$ s, increasing $|I_0|$ by 0.1 A.

analyses. The fundamental spectral envelopes computed at the utility frequency are denoted here as I_A , I_B , I_C , V_{AB} , V_{BC} , and V_{CA} .

Classical power system analysis techniques can be usefully applied to analyze spectral envelope data to develop fault signatures for machine recognition systems. For systems with a three-phase ac grid, symmetrical components [18] are a particularly useful analysis tool for developing derived streams for fault detection. The following matrix transformation produces sequence components I_0 , I_+ , and I_- from current phasors I_A , I_B , and I_C :

$$\begin{bmatrix} I_0 \\ I_+ \\ I_- \end{bmatrix} = \frac{1}{3} \begin{bmatrix} 1 & 1 & 1 \\ 1 & \alpha & \alpha^2 \\ 1 & \alpha^2 & \alpha \end{bmatrix} \begin{bmatrix} I_A \\ I_B \\ I_C \end{bmatrix}. \quad (1)$$

For a collection of phasors where I_A leads I_B which leads I_C (ABC systems), $\alpha = \exp(j2\pi/3)$. For collections of phasors in ACB sequence, $\alpha = \exp(-j2\pi/3)$. The following

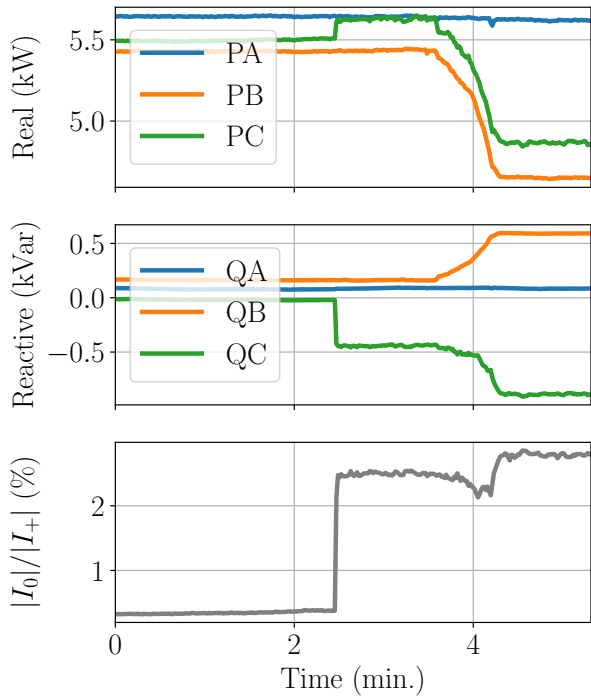


FIGURE 5. Jacket water heater failure in January 2021. Just after $t = 2$ min., phase C faults to ground. Measurement standard deviations for real power, reactive power, and $|I_0|/|I_+|$ are approximately 2 W, 3.8 var, and 0.009%, respectively.

subsections demonstrate the efficacy of derived streams for nonintrusive fault identification.

A. UNINTENTIONAL RETURN PATHS

Ungrounded three-phase delta power systems are ideally “floating” with respect to ground. They are common, for example, in shipboard microgrids [19]. However, capacitances inherent in generator construction and cable runs create high-impedance return paths from metal structures. NILMs on these systems are typically installed with three current sensors (one per phase), recording i_A , i_B , and i_C in Figure 1. The NILM then extracts current spectral envelopes I_A , I_B , and I_C . Figure 2 shows the circuit diagram of a single line-ground (LG) fault on phase B, and Figure 3 shows the circuit diagram of a double line-ground (LLG) fault on phases A and B. By Kirchoff’s current law, the total current flowing through the fault path, denoted I_G , is

$$I_A + I_B + I_C = I_G = 3I_0, \quad (2)$$

where I_0 is the zero-sequence current component as computed with Eq. (1). To illustrate, Figure 4 shows the ground fault current for both LG and LLG fault conditions (at $t = 0.1$ and $t = 0.6$ s, respectively. The top plot shows the time-domain ground current waveform through the ground fault path, and the bottom plot shows the magnitude of the resulting zero-sequence current phasor. Any time an extra return path exists for current to flow, $|I_0|$ will be nonzero. Accordingly,

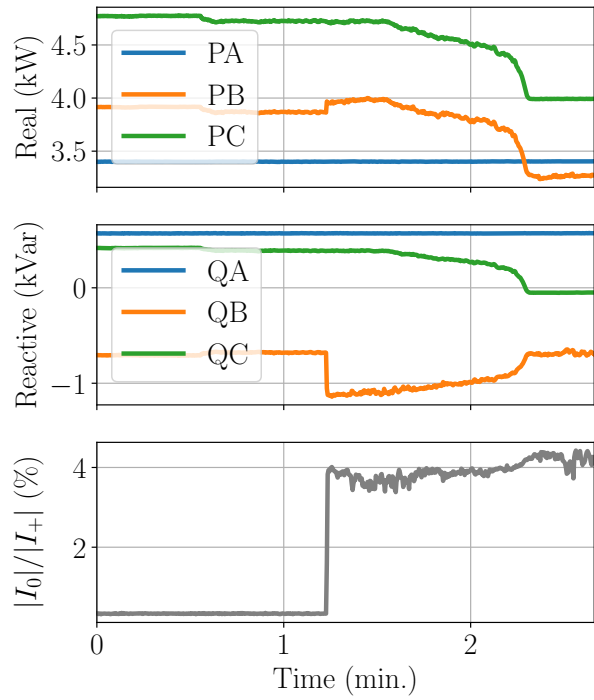


FIGURE 6. Jacket water heater failure in April 2021. Just after $t = 1$ min., phase B faults to ground. Measurement standard deviations for real power, reactive power, and $|I_0|/|I_+|$ are approximately 0.8 W, 1 var, and 0.005%, respectively.

an estimate of this “unexpected” current serves as a derived stream that can alert a monitoring system to deviations from the assumed three-wire topology, thus indicating a fault.

Figure 5 and Figure 6 show power data collected by a NILM during two three-phase heater faults described in [13], [20]. These heater faults occurred on a 270’ US Coast Guard cutter after substantial corrosion degraded the cladding on the heating elements, causing a line-to-ground fault. The bottom two plots show $|I_0|$ as a percentage of $|I_+|$. Clear step changes in this stream are correlated with the instant the ground fault occurs and creates an extra return path for current.

B. PHASE IMBALANCES

Next, consider the line-to-line voltage phasors V_{AB} , V_{BC} , and V_{CA} . Inherent to this delta measurement configuration is that these three measurements must sum to zero. This is easily shown:

$$(V_A - V_B) + (V_B - V_C) + (V_C - V_A) = 0. \quad (3)$$

Thus, the zero-sequence voltage component V_0 will always be measured as zero by a delta-connected monitoring system. The negative- and positive-sequence components reveal whether the voltage supply phasors form a balanced set, i.e. equal magnitudes and spaced 120 degrees apart in phase. A completely balanced set of voltage phasors will result in a V_- of zero. The voltage unbalance factor of a system provides a useful metric of the severity of unbalanced voltages [21]. This

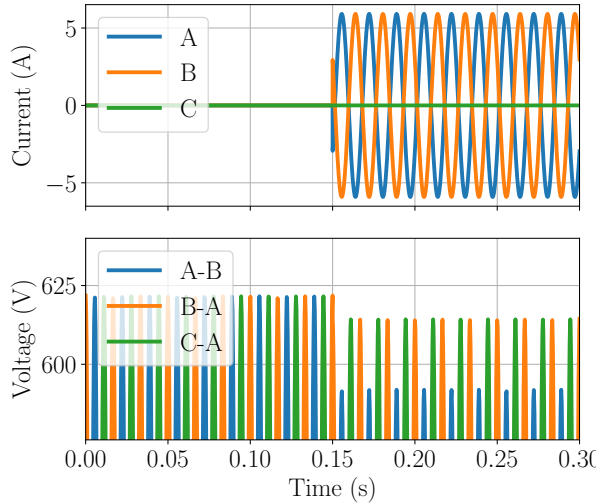


FIGURE 7. Voltage unbalance caused by a large single-phase load connected across phases A and B. At $t = 0.15\text{s}$, a load is connected across phases A and B, drawing currents through phases A and B. As these currents pass through the 2.5Ω source impedance, they cause an unbalanced voltage drop, measured at the load.

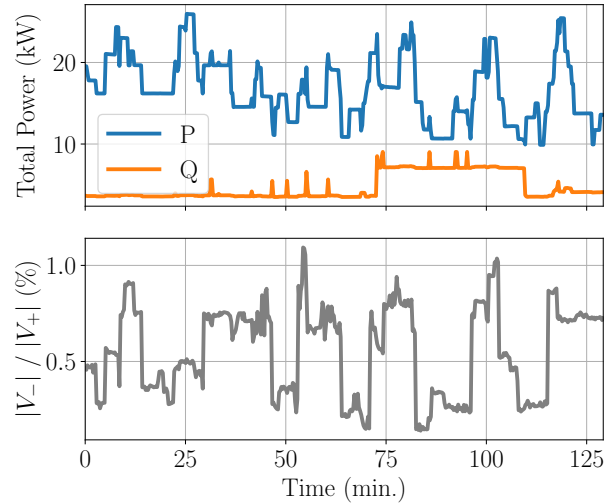


FIGURE 8. Unbalance factor stream over two hours on a shipboard microgrid. Large changes in the unbalance factor correspond to large single-phase loads energizing and de-energizing.

metric is defined as $|V_-|/|V_+|$, such that zero corresponds to a balanced set of voltages. An unbalanced set of voltages could be due to faulty generation or distribution. However, unbalanced voltages also result from unbalanced loads [22]. Unbalanced loads draw unbalanced currents. When these currents flow through source impedances, they result in unbalanced voltages seen at the point of load or monitoring. To illustrate this, Figure 7 shows the line-to-line voltages and phase currents as a single-phase load is energized across phases A and B. As current passes through the per-phase source impedance of 2.5Ω , the three line-to-line voltages drop in amplitude. Due to the unbalanced line currents, the A-B voltage drops much more than the B-C and C-A voltages. Figure 8 shows total real and reactive power and the voltage unbalance factor on a maritime power system over two hours. Large swings in the voltage unbalance factor correspond to operation of large single-phase loads. Voltage unbalance factors above 5% are considered severe by IEEE Standard 1159 [23], but unbalance factor limits are often set between 1% and 2% [24]. At times, the value of the voltage unbalance factor in Figure 8 exceeds 1%, indicating that single-phase loads significantly unbalance this microgrid's voltage.

In addition to creating power quality problems, unbalanced voltages pose a unique problem for power monitoring. When balanced loads energize on a system with unbalanced voltages, their current signatures will be unbalanced. This creates ambiguity in both manual and automated identification and diagnostics of loads through electrical data. To demonstrate, an example circuit is shown in Figure 9. If this grid has negligible source impedance (i.e., R_s and X_s are close to zero), the voltages seen by the load and the NILM will be balanced. However, all physical grids contain some non-zero

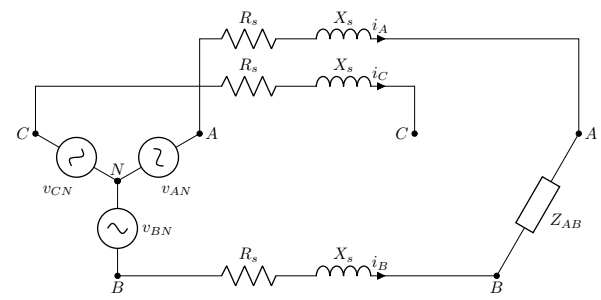


FIGURE 9. Ungrounded power system with a large load unbalance and source impedance.

source impedance. In particular, microgrids with “smaller” generation closely matched to the peak system load may contain higher per-unit source impedances than the terrestrial grid [25]. Suppose, for example, that a balanced three-phase resistive load turns on after a large single-phase load has turned on. On a hypothetical “ideal” grid with no source impedance, the change in aggregate currents due to this load would be balanced. In practice, however, the voltage applied to the load is unbalanced by the single-phase load and the source impedance. Therefore, the resulting step change in currents i_A , i_B , and i_C will also be unbalanced. This is shown in the top plot in Figure 10: at $t = 3\text{s}$ a single-phase 100Ω resistive load turns on across phases A and B. At $t = 5\text{s}$ a balanced delta-connected resistive load of 120Ω per phase turns on. The resulting transient in power spectral envelopes is shown in the left plot of Figure 11. The mean value of each phase's power real power consumption around $t = 4\text{s}$ is subtracted for clarity. Due to the single-phase load, the real power consumed by each phase of this load is out of balance. However, at $t = 10\text{s}$, the single-phase load is off while the

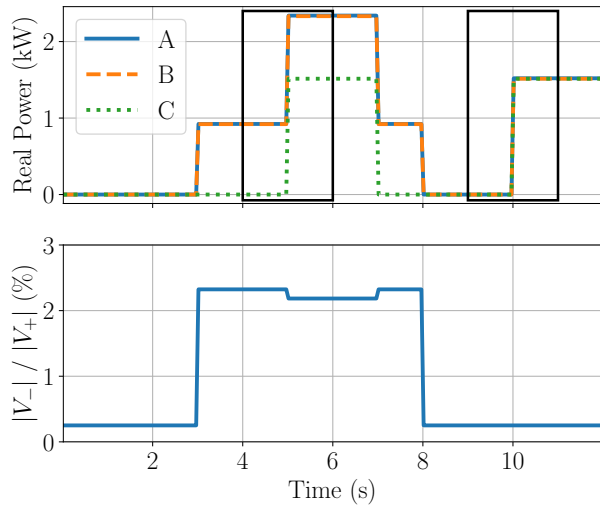


FIGURE 10. Real power and voltage unbalance factor plotted over time as a balanced and unbalanced load turn on and off.

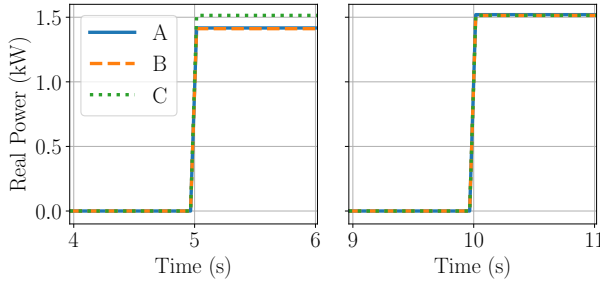


FIGURE 11. Power transients seen by a NILM corresponding to the regions in Figure 10 marked with black rectangles. Due to the presence of the single-phase load in the transient on the left, the balanced load appears unbalanced.

balanced delta load is turned on. The resulting transient is shown in the right plot of Figure 11. Here, the load's power consumption is balanced across all three phases as expected.

This imbalance is problematic for any machine monitoring system working to detect faults or pathologies, because it introduces uncertainty into key features used for identification and diagnostics. The missing link is that the power system's effective topology changed when the single-phase load was energized. The previously balanced set of voltages at the load became an unbalanced set, and the balanced load's signature changed accordingly. However, a nonintrusive monitoring system has access to measurements of these voltages, meaning it should be able to infer this system change. To do so, it can derive a stream representing the amount of unbalance in the voltage waveform set. The voltage unbalance factor (VUF) for this demonstration is shown in the bottom plot in Figure 10. Two critical pieces of information stand out. First, when the balanced load turned on at $t = 5\text{s}$, the VUF was relatively large (over 2%). This indicates to the NILM that the power system's effective topology is not a balanced voltage

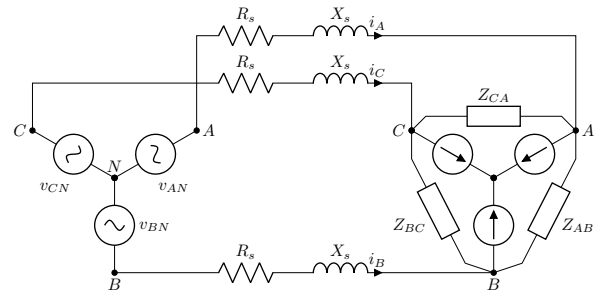


FIGURE 12. Ungrounded power system with a large fifth-harmonic current draw.

set. Second, the VUF decreases when the balanced load turns on at $t = 5\text{s}$. This means that the system became more balanced when the load turned on, rather than less. These two observations allow a NILM to recognize that the unbalanced currents are a result of changing grid conditions, rather than a changing load.

With reasonable assumptions about the character of the load, a NILM can compensate for unbalanced voltages. For example, the elevated VUF values may allow the NILM to safely assume that a balanced load was energized but in an unbalanced voltage environment. From line-to-line voltage and phase current measurements, a NILM can construct the following overdetermined linear system:

$$\begin{bmatrix} V_{AB} - V_{CA} \\ V_{BC} - V_{AB} \\ V_{CA} - V_{BC} \end{bmatrix} = \begin{bmatrix} I_A \\ I_B \\ I_C \end{bmatrix} Z_\Delta, \quad (4)$$

where Z_Δ is the per-phase delta impedance of the load. Using least-squares optimization, Z_Δ can be estimated as the following:

$$\frac{I_A^*(V_{AB} - V_{CA}) + I_B^*(V_{BC} - V_{AB}) + I_C^*(V_{CA} - V_{BC})}{|I_A|^2 + |I_B|^2 + |I_C|^2}. \quad (5)$$

Intuitively, this corresponds to the average complex power across each phase divided by the average magnitude-squared phase current. This approximation of Z_Δ can be converted to the equivalent per-phase wye impedance as $Z_Y = Z_\Delta/3$. Finally, “compensated” power spectral envelopes for each phase $\phi \in \{A, B, C\}$ can be computed as follows:

$$P_\phi + jQ_\phi = \frac{V_{rms}^2}{Z_Y^*}, \quad (6)$$

where V_{rms} is the rms line-to-neutral system voltage.

C. HARMONIC DISTORTION

The final power quality measurement example is the presence of harmonics in a power system's waveforms. Harmonics in line currents can cause equipment faults [26]. A NILM is well suited to detect anomalous harmonic signatures. However, just as unbalanced loads create unbalanced signatures, loads with high harmonic currents can affect the harmonic signature of otherwise harmonic-free loads.

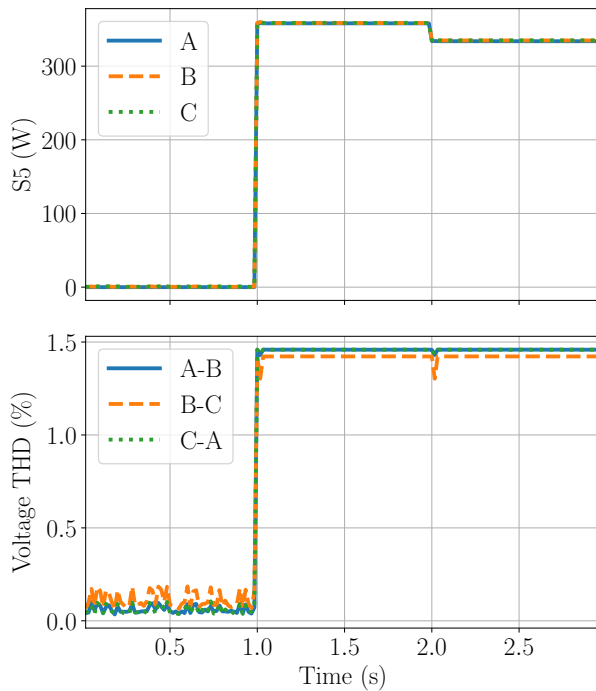


FIGURE 13. Apparent fifth harmonic power spectral envelopes and total harmonic distortion for the grid shown in Figure 12.

To illustrate, Figure 12 shows an ungrounded power system with a load modeled as current sources of 60 Hz and 300 Hz (fifth harmonic) sinusoids that energize at $t = 1\text{s}$. At $t = 2\text{s}$, a delta-connected resistive load is energized. The resulting fifth harmonic spectral envelope magnitudes (denoted S_5) are shown in Figure 13. Two step changes are visible in the S_5 stream: one at $t = 1\text{s}$ when the harmonic load is turned on and one at $t = 2\text{s}$ when the resistive load is turned on. A NILM will perceive this as two load events containing harmonic content. However, the resistive load is not drawing any harmonics on its own. Instead, the harmonic currents are divided between the source impedance and the resistive load. The NILM can derive a new stream from aggregate measurements to clarify this situation. There exist many metrics for harmonic distortion in waveforms [27]. These typically use magnitudes of harmonic and fundamental components of a waveform. They therefore can be easily computed to a desired degree of accuracy by saving a number of harmonic coefficients in spectral envelope computation. As an example, consider total harmonic distortion (THD). For a spectral envelope V with harmonic coefficients V_n , where n is the harmonic order, the total harmonic distortion of V can be computed as follows:

$$\text{THD}_V = \frac{\sqrt{\sum_{n \neq 1} |V_n|^2}}{|V_1|}. \quad (7)$$

The THD of the line-to-line voltage waveforms is shown in the bottom plot of Figure 13. Notably, there is only one

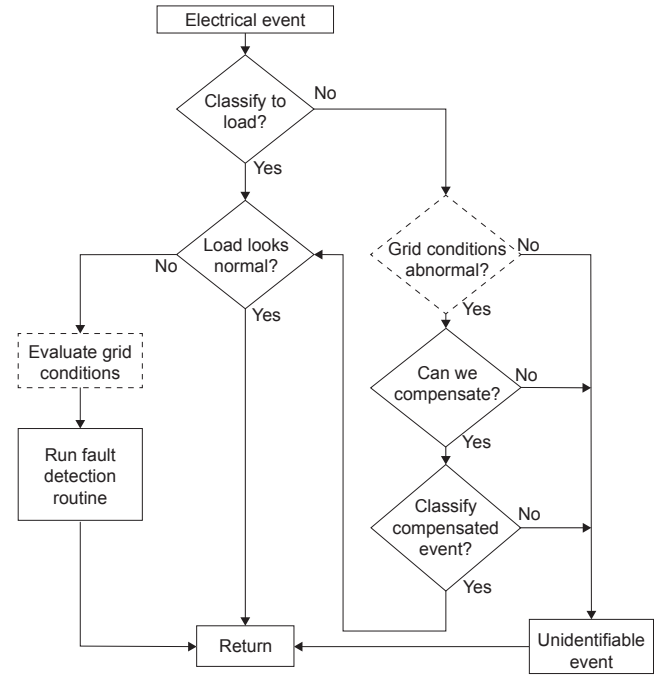


FIGURE 14. Flowchart for automated load identification and diagnostics. The dashed components show where derived streams integrate into the framework.

significant step change, which correlates with the harmonic load energizing at $t = 1\text{s}$. Since this derived stream remains constant when the resistive load turns on, it can inform a NILM that the load at $t = 2\text{s}$ was not the perpetrator of the harmonic distortion in the voltage waveforms.

IV. IMPLEMENTATION AND DEMONSTRATION

This section explains how to incorporate derived streams into a NILM's automatic fault detection procedure. Real shipboard microgrid data with faulty load operation provides a case study. Ship power systems are ideal for testing this technique, since they naturally become microgrids when underway. A ship's grid may employ as few as one or two generators, resulting in a higher source impedance compared to the terrestrial grid. They also contain a well understood set of equipment critical to life at sea, making timely detection of anomalies such as ground faults crucial [28]. However, these techniques are not limited to shipboard power systems and loads, and scale favorably to larger systems due to the aggregate nature of nonintrusive sensing. The following procedure can be generally performed on loads with faulty behavior parameterized by circuit models.

A. AUTOMATIC IDENTIFICATION AND DIAGNOSTICS

Each time it records an electrical event, a NILM performing fault detection and diagnostics must accomplish two tasks: load identification and condition assessment. These two tasks complicate each other, since a faulty load may also be an unrecognizable load. Performing both tasks is done with some variation of the process shown in Figure 14. As a NILM

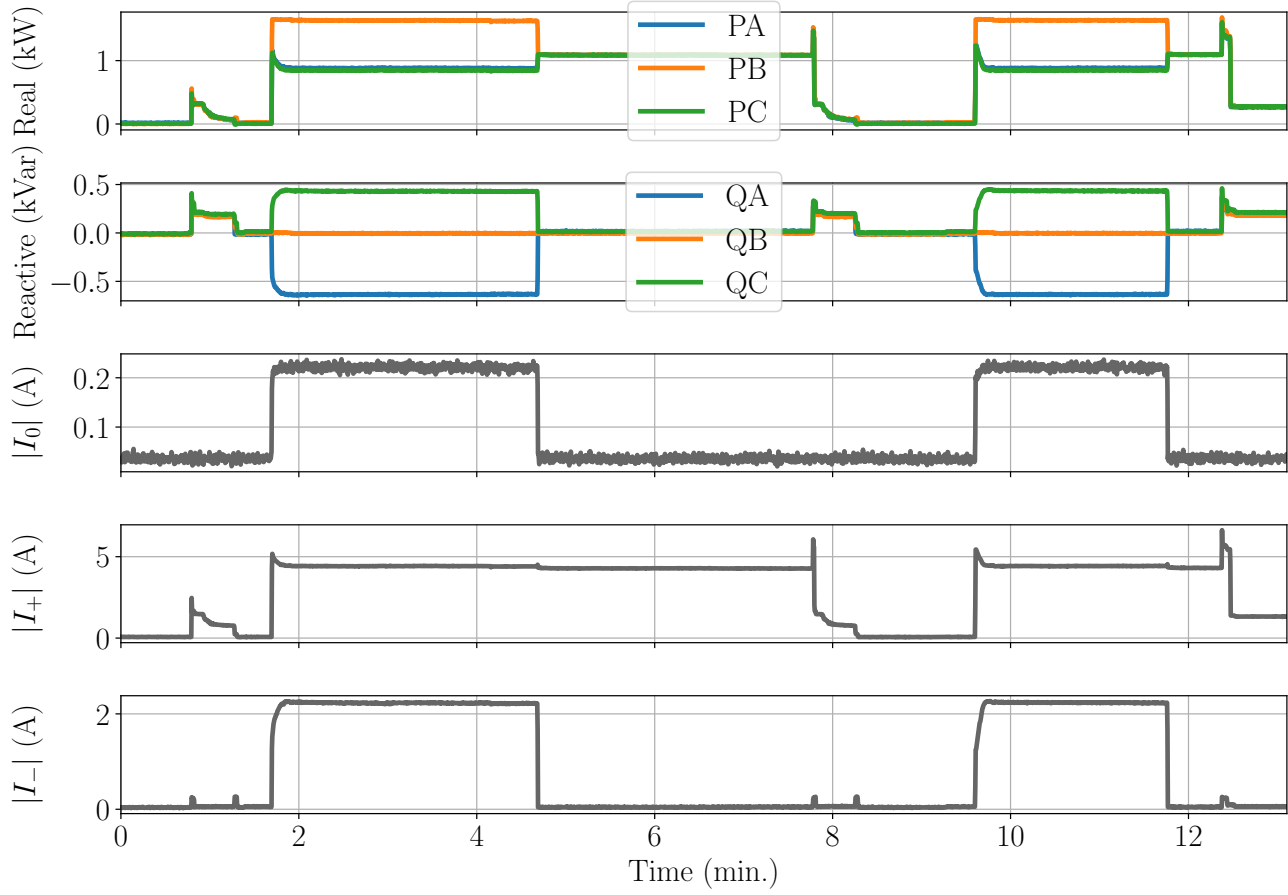


FIGURE 15. Dishwasher real and reactive power streams and zero-sequence, positive-sequence, and negative-sequence current magnitude streams recorded by a NILM on a real faulted power system. Ground faults from a broken water heater at $t = 2$ min. and $t = 10$ min. result in noticeable step changes in the derived $|I_0|$ stream.

records an electrical event, it first seeks to classify it to a known load (denoted as “Classify to load?” in Figure 14). This can be done with data-driven techniques of any desired complexity, from nearest-neighbor matching to artificial neural network classifiers. If this task, referred to here as “initial classification” is successful, the NILM should assess whether the load event looks reasonably normal (“Load looks normal?”). This may be done by comparing with past “exemplar” events known to be healthy. If the load event appears healthy, there is nothing remaining to do (“Return”). However, if the load event looks abnormal, the NILM should evaluate the conditions of the grid when the event occurred (“Evaluate grid conditions”). These conditions are revealed through the derived streams at the time of the load event, and can be checked against a threshold value calibrated for normal operation. Once these conditions are sampled, the event’s electrical data and the grid conditions are supplied to a fault estimation model for the load (“Run fault detection routine”).

If initial classification was unsuccessful, the NILM should examine the conditions of the grid using derived streams (“Grid conditions abnormal?”). If the grid conditions are

normal, then the load event cannot be classified yet (“Unidentifiable event”). Subsequent data or human intervention may allow the event to be classified later. If the grid conditions are abnormal, the NILM may be able to compensate the event’s signature using the observed grid conditions (“Can we compensate?”). If the event can be compensated and then classified to a load (“Classify compensated event?”), the NILM continues this process, checking if the load appeared normal (“Load looks normal?”).

B. SHIPBOARD CASE STUDY

Several intermittent ground faults were detected on US Coast Guard cutter William Chadwick, a 154' Fast Response Cutter homeported in Boston, MA. These faults, detected with the ship’s machinery control system (MCS), proved elusive for the crew to troubleshoot since they only lasted around a minute each time. Although the times of each ground fault occurrence were logged in the MCS, they could not be correlated to individual electrical events due to the lack of high-bandwidth power monitoring. To investigate, a portable nonintrusive load monitor was temporarily installed on the

TABLE 2. Inferred values of phase-to-ground impedances for the three-phase dishwasher heater in multiple open-circuit configurations, using the electrical signature at $t = 2$ min. in Figure 15. All values are in ohms. Bold values represent physically implausible parameter values.

Open elements	R_A	X_A	R_B	X_B	R_C	X_C
None	-51	-42.6	∞	-	-64.1	34.2
AB	3	-59	60	35	-64	34
BC	-51	-43	60	-35	2	73
CA	137	-357	∞	-	539	-1089
AB, BC	3	-59	40	0	2	73
BC, CA	137	-357	60	-35	62	31
CA, AB	49	-35	60	35	539	-1089
AB, BC, CA	49	-35	40	0	62	31

ship's 440 V three-phase electrical system. Figure 15 shows the resulting real power, reactive power, and zero-sequence current magnitude streams over a 13 minute-long period in which two ground fault events were reported. Just before $t = 2$ min. and $t = 10$ min., the value of $|I_0|$ rises above 0.2 A in a sudden step change, before returning to the baseline value of around 0.04 A in another step change. These occur simultaneously with step changes in the real and reactive power streams associated with load operation. For this case, clear step changes of over 0.1 A in $|I_0|$ correspond to ground faults. However, for larger fault datasets statistical measures such as precision, recall, accuracy, F1 scores, and correlation coefficients can be used to evaluate classification performance [11].

To diagnose this fault, the NILM first would attempt to classify this load using the turn-on events around $t = 2$ min. and $t = 10$ min. The corresponding step change in power features at $t = 2$ min. is shown below:

$$\begin{bmatrix} \Delta P_A \\ \Delta P_B \\ \Delta P_C \end{bmatrix} = \begin{bmatrix} 867 \\ 1610 \\ 830 \end{bmatrix} W, \quad \begin{bmatrix} \Delta Q_A \\ \Delta Q_B \\ \Delta Q_C \end{bmatrix} = \begin{bmatrix} -623 \\ 2 \\ 418 \end{bmatrix} var. \quad (8)$$

This signature would not match any known load on the cutter's electrical grid, so initial classification based on power features would fail. This is illustrated graphically in Figure 16, showing how feature space-based NILM methods struggle with faulty loads such as this heater. However, directly before this event, at around $t = 1$ min., a dishwasher pump turns on and then off, corresponding with a sanitizing cycle in the galley dishwasher. Using finite state machine modeling, a NILM could infer that the unidentified event was due to the water heater in the dishwasher. The NILM would then evaluate whether this load signature is normal and would quickly conclude that it is not. This heater is composed of three delta-connected heating elements, each with a resistance of 120Ω . The expected power trace, therefore, should be a step change of $(440V)^2/120\Omega \approx 1613W$ for each phase's real power, and unchanged reactive power on each phase.

Finally, the NILM can use the event's power signature and the grid conditions to uncover the type of fault occurring.

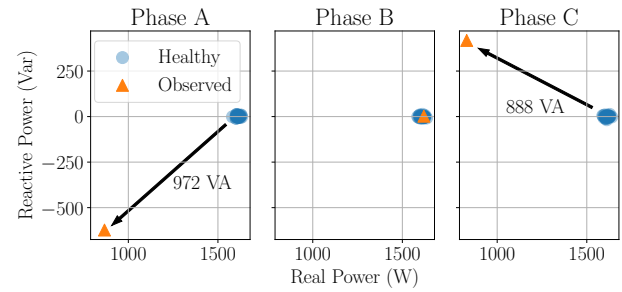


FIGURE 16. Steady-state real and reactive power feature spaces for each heater phase. Existing NILM methods seek to identify an observed load by matching its feature space signature to a cluster associated with a known load. The blue cluster represents simulated healthy signatures for the heater in Section IV-B, and the orange triangle shows the signature described in Eq. (8). The orange triangle appears in vastly different regions of the feature space than the blue healthy cluster, meaning traditional load recognition will struggle with this signature.

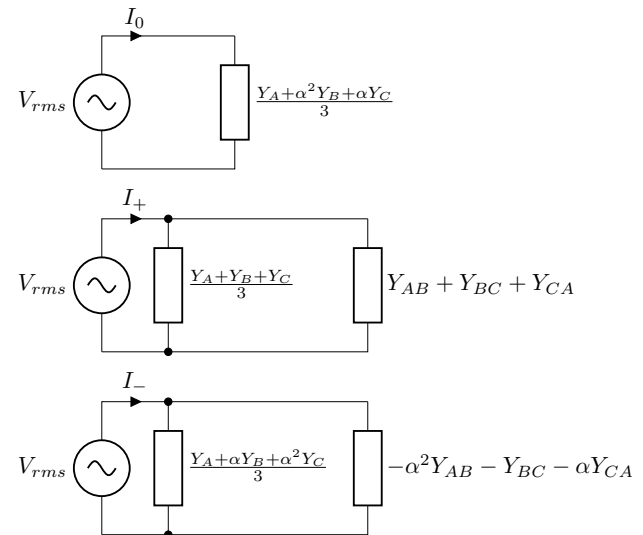


FIGURE 17. Equivalent symmetrical component impedance model, derived from Eq. (10).

To narrow the search space, the NILM would start from the premise that at least one phase in this load is faulted to ground due to the high $|I_0|$ correlated with its operation. The remaining search space includes the following parameters:

- Which phases are faulted to ground, and through what impedances?
- Which, if any, heating elements are open-circuited?

Writing out the admittance matrix \mathbf{Y} such that $\mathbf{Y}\mathbf{V}_{abc} = \mathbf{I}_{abc}$ yields

$$\begin{bmatrix} Y_A + Y_{AB} + Y_{CA} & -Y_{AB} & -Y_{CA} \\ -Y_{AB} & Y_B + Y_{AB} + Y_{BC} & -Y_{BC} \\ -Y_{CA} & -Y_{BC} & Y_C + Y_{BC} + Y_{CA} \end{bmatrix}. \quad (9)$$

Here, Y_A , Y_B , and Y_C are the fault admittances from each phase to ground, and Y_{AB} , Y_{BC} , and Y_{CA} represent the line-to-line admittance of each heating element. Rewriting this matrix

form of Ohm's law with symmetrical components results in the following:

$$\mathbf{AYA}^{-1} \begin{bmatrix} V_0 \\ V_+ \\ V_- \end{bmatrix} = \begin{bmatrix} I_0 \\ I_+ \\ I_- \end{bmatrix}. \quad (10)$$

Here, \mathbf{A} is the transformation matrix from phase to symmetrical component quantities:

$$\mathbf{A} = \frac{1}{3} \begin{bmatrix} 1 & 1 & 1 \\ 1 & \alpha & \alpha^2 \\ 1 & \alpha^2 & \alpha \end{bmatrix}, \quad (11)$$

and $\alpha = \exp(j2\pi/3)$ on an ABC system or $\exp(-j2\pi/3)$ on an ACB system. An equivalent circuit showing the values of I_0 , I_+ , and I_- is shown in Figure 17. Using numerical or algebraic techniques, the values of Y_A , Y_B , and Y_C can be estimated using the NILM's measurements of the sequence voltages and currents and postulated values of Y_{AB} , Y_{BC} , and Y_{CA} . For this analysis, each of these values can either be $1/(120\Omega)$ (healthy) or 0 (open-circuited). Thus, there are 8 possible cases, 7 of which include open-circuit failures. For each of these cases, solving Eq. (10) for Y_A , Y_B , and Y_C yields the values in Table 2. These values of R and X are the real and imaginary parts, respectively, of the line-to-ground impedances solved for by Eq. (10) (i.e., $R_A + jX_A = 1/Y_A$). Notably, for some of these rows (None, AB, and BC), their inferred values contain negative resistances, which are clearly impossible. These cases can immediately be eliminated from consideration. In addition, several rows have positive values of X, which would correspond to inductive fault impedances to ground. For this case study, these are implausible since the ship's hull is capacitively grounded. This leaves only one possible case, where heating element CA is open. In this case, phase A is inferred to be connected to ground with a resistance of 137Ω and a capacitance of $7.43\mu F$. Phase B is inferred to be connected to ground with a resistance of 539Ω and a capacitance of $2.44\mu F$.

Once the faulty heating element was identified, it was removed, revealing heavy degradation. In Figure 18 severe damage from corrosion can be seen, as well as two exposed wires from an open-circuited heating element. These wires, corresponding to phases A and C, would have been exposed to water in the dishwasher, causing the ground fault. This matches the conclusions from the previous fault analysis, enabled by the derived streams. This technique can be applied to different grid conditions, load types, and transient conditions by modifying the fault detection routine and selection of derived streams. For example, on a wye grid with a neutral point, zero-sequence current can be benign when line-to-neutral loads are connected to the system, and therefore this derived stream may not be as applicable for evaluating grid conditions.

V. CONCLUSION

Unrecognizable electrical events may be due to faulted loads or due to abnormal grid conditions. This work's key findings

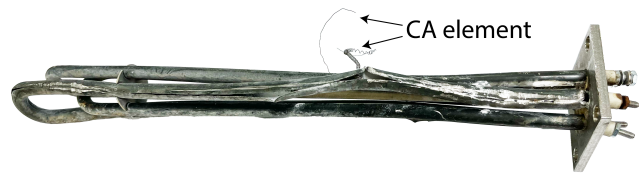


FIGURE 18. Faulty dishwasher heater from USCGC William Chadwick. One of the elements is clearly open-circuited. The two exposed wires have escaped their cladding, causing a ground fault.

show that a NILM has access to the measurements necessary to discern the two cases. The implications of this study are that a NILM can use derived streams to reconstruct the identity and condition of an otherwise unidentifiable load event. Although classical power system diagnostic indicators are used as derived streams in this work, the presented techniques are by no means limited to these. Limitations of the nonintrusive approach include difficulty in disaggregating identical loads without additional sensing. In addition, these nonintrusive techniques are strongly benefited when the electrical system is well characterized and physically understood, and disadvantaged when it is not. Future research directions include developing unsupervised techniques to apply similar fault detection techniques on partially characterized or uncharacterized electrical systems.

ACKNOWLEDGMENTS

We gratefully acknowledge the crews of USCGC William Chadwick, USCGC Marlin, and USCGC Spencer. We also gratefully acknowledge Prof. Daisy Green for her extensive work and advice on shipboard nonintrusive load monitoring. We gratefully acknowledge the support of the Office of Naval Research NEPTUNE program.

REFERENCES

- [1] G. Fenza, M. Gallo, and V. Loia, "Drift-aware methodology for anomaly detection in smart grid," *IEEE Access*, vol. 7, pp. 9645–9657, 2019.
- [2] D. H. Green, A. W. Langham, D. W. Quinn, T. C. Krause, S. R. Shaw, and S. B. Leeb, "Energy disaggregation of stochastic power behavior," *IEEE Access*, vol. 10, pp. 117985–117999, 2022.
- [3] P. A. Lindahl, M. T. Ali, P. Armstrong, A. Aboulian, J. Donnal, L. Norford, and S. B. Leeb, "Nonintrusive load monitoring of variable speed drive cooling systems," *IEEE Access*, vol. 8, pp. 211451–211463, 2020.
- [4] A. W. Langham, T. C. Krause, D. H. Green, and S. B. Leeb, "Multistream power monitoring for energy systems," *IEEE Transactions on Smart Grid*, vol. 15, no. 5, pp. 4850–4860, 2024.
- [5] N. Shabbir, R. Ahmadiahangar, A. Rosin, J. Kilter, and J. Martins, "Development of realtime co-simulation platform harnessing consumer energy flexibility through an aggregator to provide grid support," *IEEE Transactions on Consumer Electronics*, vol. 70, no. 4, pp. 6641–6652, 2024.
- [6] N. Yang, Y. Wang, Y. Zhang, and D. Yuan, "Non-intrusive load monitoring for energy management in smart grids incorporating evs," *IEEE Transactions on Consumer Electronics*, pp. 1–1, 2024.
- [7] A. W. Langham, D. H. Green, and S. B. Leeb, "Resolution analysis for power system measurement and transient identification," *IEEE Transactions on Instrumentation and Measurement*, vol. 71, pp. 1–10, 2022.
- [8] P. A. Schirmer and I. Mporas, "Non-intrusive load monitoring: A review," *IEEE Transactions on Smart Grid*, vol. 14, no. 1, pp. 769–784, 2023.
- [9] R. Jiao, C. Li, G. Xun, T. Zhang, B. B. Gupta, and G. Yan, "A context-aware multi-event identification method for nonintrusive load monitoring," *IEEE Transactions on Consumer Electronics*, vol. 69, no. 2, pp. 194–204, 2023.

- [10] E. Azizi, M. T. H. Beheshti, and S. Bolouki, "Appliance-level anomaly detection in nonintrusive load monitoring via power consumption-based feature analysis," *IEEE Transactions on Consumer Electronics*, vol. 67, no. 4, pp. 363–371, 2021.
- [11] D. H. Green, A. W. Langham, R. A. Agustin, D. W. Quinn, and S. B. Leeb, "Adaptation for automated drift detection in electromechanical machine monitoring," *IEEE Transactions on Neural Networks and Learning Systems*, vol. 34, no. 10, pp. 6768–6782, 2023.
- [12] D. H. Green, S. R. Shaw, P. Lindahl, T. J. Kane, J. S. Donnal, and S. B. Leeb, "A multiscale framework for nonintrusive load identification," *IEEE Transactions on Industrial Informatics*, vol. 16, no. 2, pp. 992–1002, 2020.
- [13] D. H. Green, P. A. Lindahl, and S. B. Leeb, "Three-phase electrical measurement representations for nonintrusive load diagnostics," *IEEE Open Journal of Instrumentation and Measurement*, vol. 1, pp. 1–14, 2022.
- [14] A. W. Langham, A. Moeller, D. W. Quinn, T. C. Krause, D. H. Green, and S. B. Leeb, "Securable networks for nonintrusive sensor fusion," *IEEE Transactions on Instrumentation and Measurement*, vol. 72, pp. 1–13, 2023.
- [15] A. Faustine and L. Pereira, "Applying symmetrical component transform for industrial appliance classification in non-intrusive load monitoring," in *ICASSP 2023 - 2023 IEEE International Conference on Acoustics, Speech and Signal Processing (ICASSP)*, 2023, pp. 1–5.
- [16] X. F. St-Onge, J. Cameron, S. Saleh, and E. J. Scheme, "A symmetrical component feature extraction method for fault detection in induction machines," *IEEE Transactions on Industrial Electronics*, vol. 66, no. 9, pp. 7281–7289, 2019.
- [17] J. Paris, J. S. Donnal, Z. Remscrim, S. B. Leeb, and S. R. Shaw, "The sinefit spectral envelope preprocessor," *IEEE Sensors Journal*, vol. 14, no. 12, pp. 4385–4394, 2014.
- [18] J. L. Kirtley, "System analysis and protection," in *Electric Power Principles*. John Wiley & Sons, Ltd, 2020, ch. 10, pp. 181–211.
- [19] N. Doerry, "Naval power systems: Integrated power systems for the continuity of the electrical power supply," *IEEE Electrification Magazine*, vol. 3, no. 2, pp. 12–21, 2015.
- [20] D. H. Green, D. W. Quinn, S. Madden, P. A. Lindahl, and S. B. Leeb, "Nonintrusive measurements for detecting progressive equipment faults," *IEEE Transactions on Instrumentation and Measurement*, vol. 71, pp. 1–12, 2022.
- [21] H. Wen, D. Cheng, Z. Teng, S. Guo, and F. Li, "Approximate algorithm for fast calculating voltage unbalance factor of three-phase power system," *IEEE Transactions on Industrial Informatics*, vol. 10, no. 3, pp. 1799–1805, 2014.
- [22] M. Savaghebi, A. Jalilian, J. C. Vasquez, and J. M. Guerrero, "Autonomous voltage unbalance compensation in an islanded droop-controlled microgrid," *IEEE Transactions on Industrial Electronics*, vol. 60, no. 4, pp. 1390–1402, 2013.
- [23] "IEEE recommended practice for monitoring electric power quality," *IEEE Std 1159-2019 (Revision of IEEE Std 1159-2009)*, pp. 1–98, 2019.
- [24] F. Ghassemi and M. Perry, "Review of voltage unbalance limit in the gb grid code cc. 6.1. 5 (b)," *National Grid, Report*, pp. 14–58, 2014.
- [25] D. Kumar and F. Zare, "A comprehensive review of maritime microgrids: System architectures, energy efficiency, power quality, and regulations," *IEEE Access*, vol. 7, pp. 67 249–67 277, 2019.
- [26] G. J. Wakileh, "Introduction," in *Power Systems Harmonics: Fundamentals, Analysis and Filter Design*. Berlin, Heidelberg: Springer Berlin Heidelberg, 2001, pp. 1–4.
- [27] A. Arranz-Gimon, A. Zorita-Lamadrid, D. Morinigo-Sotelo, and O. Duque-Perez, "A review of total harmonic distortion factors for the measurement of harmonic and interharmonic pollution in modern power systems," *Energies*, vol. 14, no. 20, 2021.
- [28] K.-T. Ryu and Y.-H. Lee, "Ground-fault recognition in low-voltage ships based on variation analysis of phase-to-ground voltage and neutral-point voltage," *IEEE Access*, vol. 12, pp. 123 166–123 176, 2024.



AARON W. LANGHAM (Graduate Student Member, IEEE) received the B.E.E. degree in electrical engineering from Auburn University, Auburn, AL, USA in 2018, and the M.S. and E.E. degrees in electrical engineering and computer science from the Massachusetts Institute of Technology, Cambridge, MA, USA in 2022 and 2024, respectively. He is currently pursuing the Ph.D. degree in electrical engineering and computer science at the Massachusetts Institute of Technology, Cambridge, MA, USA. His research interests include signal processing, machine learning, and IoT platforms for energy systems.



THOMAS C. KRAUSE (Graduate Student Member, IEEE) received the B.S. degree in electrical engineering from Purdue University, West Lafayette, IN, USA, in 2019, and the M.S. and E.E. degrees in electrical engineering and computer science from the Massachusetts Institute of Technology, Cambridge, MA, USA, in 2021 and 2024, respectively, where he is currently pursuing the Ph.D. degree.



STEVEN B. LEEB received the Ph.D. degree from the Massachusetts Institute of Technology, in 1993. Since 1993, he has been a member on the MIT Faculty with the Department of Electrical Engineering and Computer Science. He also holds a joint appointment with the Department of Mechanical Engineering, MIT. He is concerned with the development of signal processing algorithms for energy and real-time control applications.